Mon. Not. R. astr. Soc. (1991) **253**, 307–319

The large-scale clustering of radio galaxies

J. A. Peacock[1] and D. Nicholson[2]
[1] *Royal Observatory, Blackford Hill, Edinburgh EH9 3HJ*
[2] *Department of Astronomy, University of Edinburgh, Blackford Hill, Edinburgh EH9 3HJ*

Accepted 1991 July 8. Received 1991 June 27; in original form 1991 April 22

SUMMARY

We use an all-sky sample of radio galaxies at redshifts $z \lesssim 0.1$ to study clustering in the Universe on scales up to several hundred Mpc. The two-point correlation function for these galaxies is consistent with their high optical luminosity and location in moderately rich environments: $\xi(r) \simeq (r/11\ h^{-1}\ \mathrm{Mpc})^{-1.8}$, where $h \equiv H_0/100$ km s^{-1} Mpc^{-1}.

We discuss direct methods for obtaining the power spectrum of the density field traced by the radio galaxies, taking into account the selection function of the sample. The results of the power-spectrum analysis indicate that the distribution of radio galaxies is more uniform on very large scales than would be predicted from an extrapolation of the power-law clustering found on small scales. There is a break to an effective spectral index $n \gtrsim -0.5$ for wavelengths $\lambda \gtrsim 200\ h^{-1}$ Mpc. The variance in $\delta N/N$, σ^2, is about 0.3 for wavelengths $80 < \lambda < 200\ h^{-1}$ Mpc, and there is no concentration towards the supergalactic plane for $z \gtrsim 0.02$. We thus do not confirm suggestions made by Broadhurst *et al.* and by Tully of strong clustering on scales of $\gtrsim 100$ Mpc.

1 INTRODUCTION

Radio galaxies have an honourable history as probes of cosmological large-scale structure: some of the first evidence for large-scale isotropy came from the observed lack of clustering in the sky distribution of sources found in cm-wavelength surveys. As the culmination of a series of papers on radio-galaxy clustering, Webster (1977) was able to show that the fluctuations in radio-galaxy number density between randomly-placed cubes of side 1 Gpc were $\lesssim 3$ per cent. Scaling density perturbations as $(1+z)^{-1}$ back to last scattering at $z \simeq 1000$, this implies density fluctuations $\lesssim 10^{-4}$ at that time – which still provides a limit comparable to present observations of microwave background anisotropies on the relevant scales ($\sim 10°$).

Webster's constraint probes such large scales because he was investigating the 2D projected clustering in radio surveys. The typical redshift in these surveys is $z \simeq 1$, so that projection effects decrease sensitivity to clustering on smaller scales very severely. Nevertheless, Webster's work emphasizes the utility of radio galaxies for work on large-scale structure; the simplicity and uniformity of source selection makes these objects excellent statistical probes. This paper therefore considers the three-dimensional distribution of radio galaxies, based on a redshift survey which we have recently completed. Our principal results are not only to obtain the first detection of clustering of these objects on $\sim$ 10 Mpc separations, but also to constrain clustering on larger ($\gtrsim 100$ Mpc) scales. This region of the clustering spectrum has been of especial interest recently through suggestions that the galaxy distribution may display large inhomogeneities on these scales (Tully 1986, 1987; Broadhurst *et al.* 1990). Existing optical redshift surveys lack the depth to form a fair sample of such fluctuations, so our sample has an important role to play here.

The plan of the paper is as follows: we describe the database in Section 2. Section 3 performs the autocorrelation function analysis. Section 4 considers superclustering in the radio-galaxy distribution, and investigates whether there is any large-scale concentration towards the supergalactic plane. In Section 5, we perform a direct power-spectrum analysis, in an attempt to constrain very large-scale clustering. Section 6 summarizes our conclusions.

2 A RADIOGALAXY REDSHIFT SURVEY

We now describe the data to be used in this paper; a full description will be given in Nicholson *et al.* (in preparation). The sample of galaxies analysed here is an approximation to the following idealized criteria: (i) flux density $S > 0.5$ Jy at 1.4 GHz; (ii) redshift $0.01 < z < 0.1$; (iii) galactic latitude $|b| > 15°$. An outline of the actual properties of the sample is given in Appendix A. We began with a list of nearly 600

candidate objects expected to have $z \lesssim 0.1$, from which spectroscopy has yielded 310 definite sample members. The remainder either now have measured $z > 0.1$ or are rather faint optically, and so are very unlikely to lie at $z < 0.1$ (radio galaxies being optical standard candles). Estimating the remaining unknown redshifts from apparent magnitude suggests that the total number with $z < 0.1$ will eventually reach 329. We have used the additional 19 objects with estimated redshifts < 0.1 in the clustering analysis, although their exclusion has little effect on the results. Fig. 1 shows the sky distribution of the sample; the aim of all-sky uniformity appears to have been achieved reasonably well. There are some 'holes' in the $z < 0.1$ sky distribution, but these contain $z > 0.1$ objects and so appear to be real, rather than the result of incompleteness in the radio survey optical identification process.

The completeness of the sample may be assessed by comparison with the known form of the local radio luminosity function $[\rho(P)]$ for elliptical galaxies, which has been derived at 1.4 GHz by Auriemma *et al.* (1977) and Windhorst (1984). For an assumed parametric form

$$\rho/[h^3\,\mathrm{Gpc}^{-3}(\Delta \log_{10} P)^{-1}] = \phi^* \left(1 + \frac{P}{P^*}\right)^{-1}, \qquad (1)$$

their results may be fitted

$$(\phi^*, P^*) = \begin{cases} (10^{5.2},\ 10^{22.1}\ h^{-2}\,\mathrm{WHz}^{-1}\,\mathrm{sr}^{-1}) & \text{Windhorst} \\ (10^{4.7},\ 10^{22.6}\ h^{-2}\,\mathrm{WHz}^{-1}\,\mathrm{sr}^{-1}) & \text{Auriemma } \textit{et al.} \end{cases} \qquad (2)$$

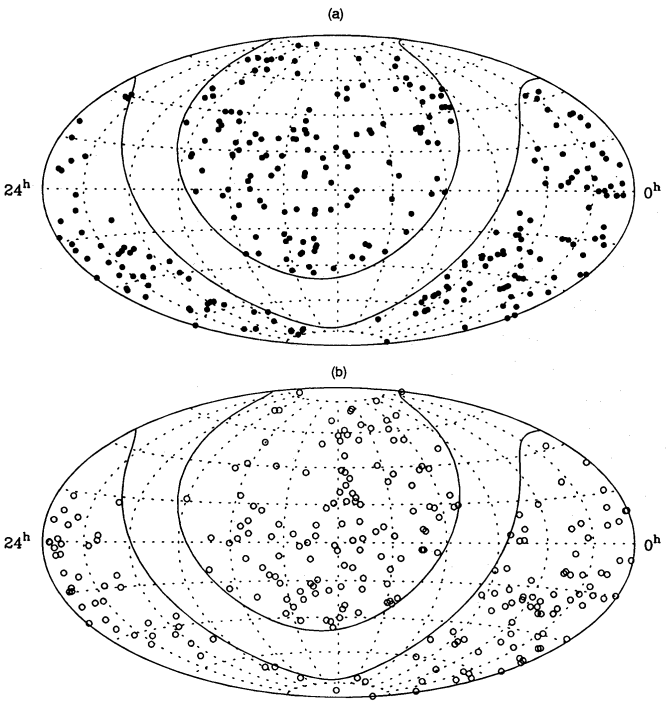

Figure 1. The sky distribution of radio galaxies in the $z < 0.1$ sample, plotted on an Aitoff equal-area projection. (a) Objects with spectroscopic redshifts; (b) all remaining objects which were initially selected as candidate sample members. All of these are either now known to have $z > 0.1$, or are very likely to have redshifts above this limit. Probably only about 20 sample members remain to be found. Note that candidates do exist in regions of the sky devoid of $z < 0.1$ sample members; these holes are not the result of incomplete searches for radio-source identifications.

This functional form is easily integrated to yield the predicted redshift distribution:

$$dn(z) = dv(z)\, N[> P(z)], \qquad (3)$$

where, for $\Omega = 1$,

$$P(z)/(h^{-2}\,\mathrm{WHz}^{-1}\,\mathrm{sr}^{-1}) = 8.569 \times 10^{25} (S/\mathrm{Jy}) \left[2\left(1 - \frac{1}{\sqrt{1+z}}\right)\right]^2 (1+z)^{1+\alpha} \qquad (4)$$

and we shall take a spectral index $\alpha = 0.8$ to be representative.

Theoretical curves for RLFs with the model parameters given above are shown in Fig. 2. As expected, incompleteness sets in at $z \simeq 0.1$, reaching a factor of about 2 by $z = 0.15$. The observed numbers of objects may seem low for $z > 0.08$, rather than 0.1, but given the structure in the redshift distribution at lower redshifts there is no clear evidence for incompleteness until we reach $z > 0.1$. The total expected numbers of sources in the redshift shell from $z = 0.01 \rightarrow 0.1$ down to the flux limit of 0.5 Jy are respectively 305 and 349 for the Auriemma *et al.* and Windhorst sets of parameters. The difference between these estimates is hardly surprising, given that the volumes of space analysed in those surveys are much smaller than that considered here. To sum up, any incompleteness in the sample would appear to be no worse than 10 per cent.

3 THE CORRELATION FUNCTION

The simplest measure of clustering is the two-point correlation function. This measures the excess probability for finding a pair in two volumes dV_1 and dV_2 separated by a distance r (throughout, we take $\Omega = 1$ and work in terms of comoving distance, so that the spatial geometry is Euclidean):

$$dP = \rho_0^2 [1 + \xi(r)]\, dV_1\, dV_2. \qquad (5)$$

In practice, this statistic is usually measured by creating a random catalogue much larger in size than the sample under

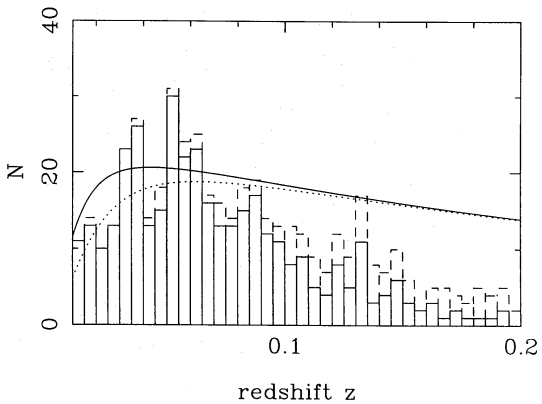

Figure 2. The redshift distribution for the sample (solid histogram), with an estimate of the expected distribution of the remaining candidates. The two lines show the expected distribution for a uniform flux-density limit of 0.5 Jy at 1.4 GHz, according to the luminosity functions of Auriemma *et al.* (1977, dotted line) and Windhorst (1984, solid line). The sample appears reasonably complete to its design limit of $z = 0.1$, but rapidly becomes heavily incomplete thereafter.

study, and by counting pairs either within the two catalogues (symbolized by $\langle DD\rangle$ and $\langle RR\rangle$) or between catalogues (symbolized by $\langle DR\rangle$), giving the two estimates

$$1+\xi_1=\langle DD\rangle/\langle RR\rangle \qquad 1+\xi_2=\langle DD\rangle/\langle DR\rangle. \tag{6}$$

In both cases one is effectively measuring the expected number of pairs by Monte-Carlo integration. The second estimator is usually held to be more robust and is the version used in this work. However, similar results were obtained using ξ_1.

3.1 Simulated catalogues

An accurate estimate of $\xi(r)$ depends on understanding the sample selection effects, so that true clustering may be disentangled from variations in depth or completeness. To illustrate these problems, we have considered three different methods for generating synthetic catalogues. In order of increasing realism, these are given below.

(i) Assume uniform sky coverage with redshift homogeneity: generate a random (α, δ) pair consistent with $|b|>15°$ and choose from the list of the observed redshifts randomly.

(ii) Assume declination-dependent completeness but redshift homogeneity: select randomly from the list of observed declinations, choose a random right ascension and redshift as in (i).

(iii) Assume that both the completeness and redshift distribution vary over the sky. Select randomly from the list of observed sky coordinates and match this with a randomly chosen redshift. Because part of the real clustering pattern comes from the fact that groups of close galaxies exist, we need to smooth the sky distribution to some extent. Accordingly, random perturbations over a circle of radius θ were added to positions randomly selected from the observed set. For objects lying at $|b|<15°+\theta$, the perturbations were constrained to produce a resultant at $|b|>15°$, thus avoiding a spurious reduction in smoothed surface density near the galactic plane. The redshifts were selected, not from the whole catalogue, but from those objects within $\pm\theta$ in declination of the chosen position. Values of θ up to 20° were investigated.

Having made estimates of $\xi(r)$, we now need to consider error bars. In the absence of clustering, $\langle\xi\rangle=0$ and $\langle\xi^2\rangle=1/N_p$, where N_p is the number of independent pairs in a given radial bin (Peebles 1980). For non-zero ξ, this suggests the usual 'Poisson error bar'

$$\frac{\Delta\xi}{1+\xi}=\frac{1}{\sqrt{N_p}}. \tag{7}$$

This will usually be a lower limit to the uncertainty in ξ; Peebles (1973) shows that the right-hand side should be increased by a factor of approximately $1+4\pi nJ_3$, $4\pi J_3$ being the volume integral of ξ out to the radius of interest, and n being the number density (see also Kaiser 1986). The problem with this expression is that J_3 may be hard to estimate. It has been suggested (Ling, Frenk & Barrow 1986) that the correct errors can be estimated via the bootstrap resampling method. It seems to us that even this provides an underestimate: one is always concerned with sampling errors in the sense that large-scale variations in properties of the density field cause the area under study not to be a totally fair sample. There is no totally satisfactory way of dealing with this problem: any error bars we produce can only be lower bounds to the true errors. Here, we shall adopt the simplest method of initially presenting results with Poisson errors (without J_3 corrections), and then discuss modifications to these once we have some internal data on the likely magnitude of J_3. In practice, it will turn out that Poisson errors are a reasonable approximation up to $r\simeq 20\ h^{-1}$ Mpc.

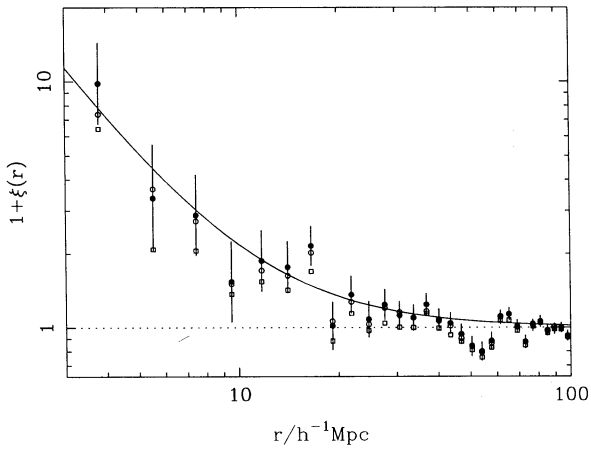

Figure 3. The two-point correlation function in redshift space, $\xi(r)$, for the whole sample. The filled points are derived using the uniform-sky random catalogues (method 1). Results for random catalogues generated using methods 2 and 3 are shown as open circles and open squares respectively. The method 3 points adopted $\theta=20°$; it is apparent that this reduces the amplitude of clustering slightly. Smaller values of θ make larger differences, but at this point we are almost certainly removing real structure from the sky distribution. The curve shows the best-fit model $\xi(r)=(r/11\ h^{-1}\ \mathrm{Mpc})^{-1.8}$. The error bars plotted are simple Poisson errors only; as discussed in the text, it is apparent that these are too small by a factor of at least 2–3 at large r.

3.2 Results

Fig. 3 plots the correlation-function results. We show $\xi(r)$ for the whole sample, illustrating the effects of different random catalogue methods on ξ. There is a tendency for the uniform-sky random catalogue (method 1) to give a slightly higher answer, and for method 3 to give the lowest answer, as might have been expected. However, unless θ is made rather smaller than the value of 20° used here, all methods of determination are consistent to well within the random errors. This was not the case in the earlier stages of this project; Peacock *et al.* (1988) presented a preliminary correlation function based on only 125 redshifts available at that time. The random catalogues then were based on method 2 – using observed declinations. Assumption of a uniform sky density yielded a much larger $\xi(r)$, as was to be expected given that different declination bands did then indeed differ greatly in completeness. The present result is much more robust.

The most striking characteristic of $\xi(r)$ is its large amplitude. The slope is not particularly well constrained, but the scalelength for unit clustering is quite well determined. Fitting a model to correlation-function data is a somewhat

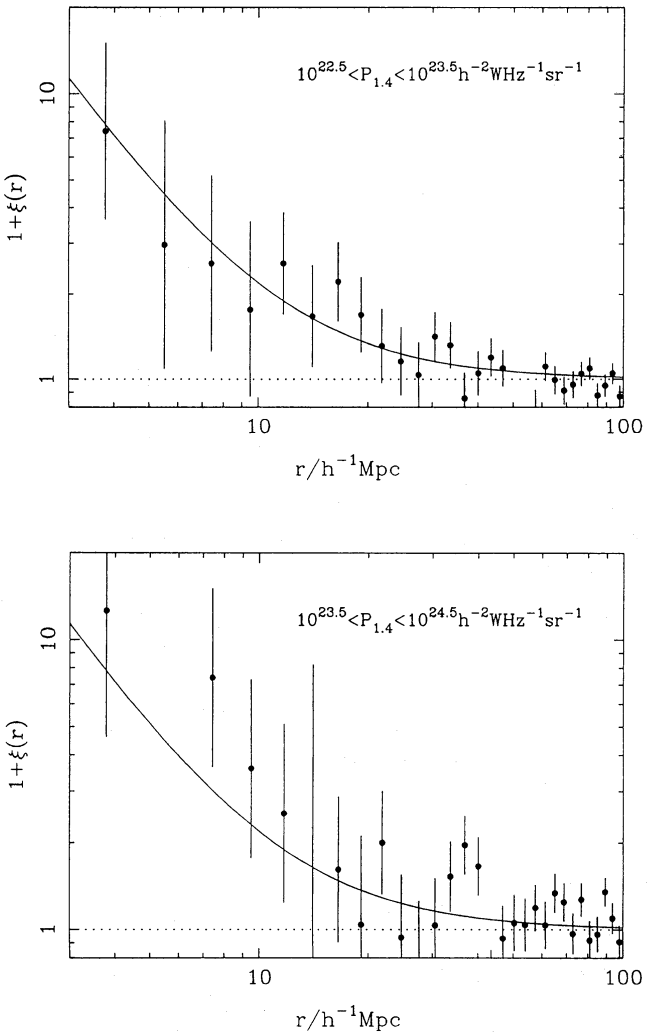

Figure 4. The two-point correlation function in redshift space, $\xi(r)$, for the sample divided into two bins of radio power. Symbols are as for Fig. 3. There appears to be no trend towards stronger clustering in the weaker power bin, contrary to suggestions from a preliminary version of the sample.

uncertain process as the various plotted points are not guaranteed to be independent. However, if we neglect this complication and simply fit the model

$$\xi(r)=(r/r_0)^{-\gamma} \tag{8}$$

to the observed data points (method 1) with Poisson errors, then one obtains $\gamma=1.8\pm0.3$ and $r_0=11.0\pm1.2\ h^{-1}$ Mpc (fitting $r<30\ h^{-1}$ Mpc only). These numbers are not very sensitive to the use of different random catalogue methods or different ranges of r. Using method (3) with $\theta=20°$ reduces r_0 by about 20 per cent; however, we have already argued that this method is likely to be subtracting real clustering signal. It thus appears that the radio galaxies are correlated about four times more strongly than normal galaxies, for which $\xi\simeq(r/5\ h^{-1}\,\mathrm{Mpc})^{-1.8}$.

We can now discuss error bars on $\xi(r)$. If we adopt the power-law model $\xi(r)=(r/11)^{-1.8}$, then the $1+4\pi nJ_3$ correction term may be estimated. The mean density of the sample is about $10^{-5.3}\ h^3\ \mathrm{Mpc}^{-3}$, in which case $4\pi nJ_3\simeq(r/77\ h^{-1}\,\mathrm{Mpc})^{1.2}$. We shall show in Section 5 that this is, if anything, an over-estimate for large r. The density is somewhat higher at low redshift, so use of the mean density may underestimate the correction by a moderate factor, because more pairs will be drawn from the high-density regions. Looking at the points with negative ξ at $r\simeq50$, one would suspect that the errors are too small at this point by a factor 2–3, which corresponds to $1+4\pi nJ_3$ with an effective n value of at most around five times higher than the mean. Nevertheless, this is still sufficiently low that the Poisson errors should be close to the truth for $r\lesssim20$, and so the detection of clustering and the determination of r_0 cannot be seriously affected. For larger scales, we prefer to rely on the power-spectrum analysis in Section 5.

In retrospect, this strength of clustering is hardly surprising, since radio galaxies are abnormal in three related ways: they are ellipticals; they are optically highly luminous; and they tend to reside in clusters. Any of these properties would give reason to expect enhanced correlations. Elliptical galaxies have long been known to possess stronger correlations: $\xi(r)$ for these is about three times larger than for galaxies in general (Davis & Geller 1976). Although luminosity segregation is a puzzlingly weak effect, there is some evidence that it may be present for galaxies with $L\gtrsim L_*$ in the sense of an enhancement of a factor about 4 in ξ (e.g. Valls-Gabaud, Alimi & Blanchard 1989; although see Phillipps & Shanks 1987 for a contrary opinion). The correlations of Abell clusters show an analogous enhancement; initial claims of a scalelength of 25 h^{-1} Mpc by Bahcall & Soneira (1983) appear to have been due to internal problems with the Abell catalogue, and a revised scalelength of 14 h^{-1} Mpc with little richness dependence is given by Sutherland (1988). Our results fit in well with such properties for galaxies in general, and indeed provide some independent confirmation for them. Radio galaxies range in luminosity from normal giant ellipticals to the largest cD galaxies (e.g. Lilly & Prestage 1987; Owen & Laing 1989) and they occupy a range of environments from poor groups to the richest clusters (Longair & Seldner 1979; Prestage & Peacock 1988, 1989; Yates, Miller & Peacock 1989; Hill & Lilly 1991). Although this spread in properties is an important fact to recognise, nevertheless on average the galaxies in our present sample will have luminosities $\bar{L}\simeq5L_*$ and Abell richnesses $\bar{R}\simeq0$; enhanced clustering is thus almost inevitable.

One caveat which merits discussion is that we have measured clustering in redshift space, which can lead to a distortion of the clustering pattern. At small separations, virialized peculiar velocities tend to smear out the highest-density regions ('fingers of God'); at large scales, conversely, peculiar velocities in the linear regime will amplify apparent perturbations. This process was analysed by Kaiser (1987), who showed that the azimuthally-averaged correlation function or power spectrum is enhanced by a factor

$$\xi_s/\xi_r=1+2\Omega^{0.6}/3+\Omega^{1.2}/5, \tag{9}$$

i.e. a factor of 28/15 for $\Omega=1$. Clearly, this cannot account for the enhanced clustering we observe; there must be real enhancements in the spatial clustering pattern. Because of this, our estimate of the clustering is less sensitive to the effects of virialized peculiar velocities than would be the case for a set of less clustered objects.

There is one important distinction between the 1988 result and the present one, however. In 1988, the clustering signal appeared to be confined to a band in radio power. At the time, this seemed to be consistent with the fact that mean cluster richness dropped around the Fanaroff–Riley (1974) borderline. However, there is no strong evidence for a luminosity dependence in the final data. Fig. 4 shows $\xi(r)$ for the sample divided in radio luminosity, and no significant trend is evident. If anything, the clustering in the high-power bin may be stronger, which would be the opposite of the effect previously claimed. In retrospect, this may not be so surprising: the later investigations of radio-galaxy cluster richnesses (Prestage & Peacock 1988, 1989; Yates *et al.* 1989; Hill & Lilly 1991) have found a smaller difference between the environments of weak and powerful radio galaxies than was suggested by Longair & Seldner (1979).

4 SUPERCLUSTERING OF RADIO GALAXIES

4.1 Possible superclusters and voids

To see directly whether the large-scale power seen here is connected with particular superclusters, one may construct a list of possible groups using the 'friends of friends' algorithm. Here, one finds sets of objects which are connected in the sense that one can move along the tree between members of the set by steps of at most some characteristic linkage radius r. Table 1 lists the results of this analysis for $r = 20\ h^{-1}$ Mpc, excluding groups consisting of fewer than four galaxies.

Somewhat discouragingly, none of these groups appear in the list of superclusters compiled by Bahcall & Soneira (1984); however, the majority of the groups defined by these authors are at higher redshift than those listed here. Much better correspondence exists with the groups found in the QDOT *IRAS* redshift survey (Saunders *et al.* 1991). Group 4 corresponds roughly to *IRAS* group S6; group 5 to *IRAS* group NH; group 7 to *IRAS* group A2; group 9 to *IRAS* group PI. It is encouraging that (with the exception of group 1) this accounts for the richer of our groups, implying that the clustering signal claimed above is indeed real. Interestingly, we find no trace in our data of the very large Abell supercluster at ($13.5^{\rm h}$, $-30°$, $z = 0.05$) pointed out by Scaramella *et al.* (1989), which also fails to appear in the *IRAS* list. This fact, plus the lack of correspondence with the Bahcall & Soneira supercluster list, may cast some doubt on the use of the Abell catalogue for investigations of large-scale structure.

Some indication of the amplitude of very large-scale perturbations is given in Table 1 by the numbers δ_{20} etc.; these indicate the fractional number contrast in spheres of radius 20, 30 and 40 h^{-1} Mpc centred on each supercluster candidate. Although the Poisson fluctuations are large, with only ~ 10 objects inside even the largest sphere, it seems clear that order unity fluctuations exist for at least some 40 h^{-1} Mpc spheres within our sample volume. For completeness, we have also looked at the distribution of void sizes in the sample. Restricting ourselves to voids which lie entirely inside the sample boundaries (and at $z < 0.07$ to exclude the lower-density outer edge of the sample), the largest voids found have radius 50 h^{-1} Mpc. Their approximate locations are 0220 − 69 ($z = 0.050$), 0330 − 08 ($z = 0.051$), 1015 − 06 ($z = 0.043$), 1030 + 09 ($z = 0.049$) and 1550 + 45 ($z = 0.051$). Again, the significance of any individual one of these is small (expected number of objects about five), but at least one must be real (indeed, the 1550 + 45 void corresponds to the *IRAS* BV void).

Table 1. 'Friends of friends' groups with pairing radius 20 h^{-1} Mpc.

Group 1
$\bar{l} = 164°$ $\bar{b} = -48°$ $\bar{z} = 0.021$
$\delta_{20} = 4.9$ $\delta_{30} = 1.4$ $\delta_{40} = 1.1$

0036+030	0.0140
0123−016	0.0177
0153+053	0.0186
0238+085	0.0214
0238+084	0.0217
0255+058	0.0234
0305+039	0.0288
0325+023	0.0302
0356+102	0.0306
2318+079	0.0111

Group 2
$\bar{l} = 128°$ $\bar{b} = -63°$ $\bar{z} = 0.043$
$\delta_{20} = 13.0$ $\delta_{30} = 2.6$ $\delta_{40} = 1.5$

0053−016	0.0436
0053−015	0.0385
0055−016	0.0444
0111+021	0.0466

Group 3
$\bar{l} = 251°$ $\bar{b} = -55°$ $\bar{z} = 0.064$
$\delta_{20} = 21.4$ $\delta_{30} = 7.2$ $\delta_{40} = 3.5$

0314−440	0.0628
0319−454	0.0633
0326−461	0.0690
0332−391	0.0626

Group 4
$\bar{l} = 226°$ $\bar{b} = -31°$ $\bar{z} = 0.034$
$\delta_{20} = 7.0$ $\delta_{30} = 1.9$ $\delta_{40} = 1.0$

0431−134	0.0364
0449−175	0.0318
0453−206	0.0343
0502−103	0.0394
0503−286	0.0381
0546−329	0.0369
0548−317	0.0326
0618−371	0.0324

Group 5
$\bar{l} = 262°$ $\bar{b} = -25°$ $\bar{z} = 0.051$
$\delta_{20} = 20.8$ $\delta_{30} = 4.9$ $\delta_{40} = 2.5$

0605−494	0.0519
0616−487	0.0465
0620−526	0.0511
0625−536	0.0539
0625−545	0.0519
0649−557	0.0492
0641−584	0.0561

Group 6
$\bar{l} = 307°$ $\bar{b} = 40°$ $\bar{z} = 0.014$
$\delta_{20} = 2.7$ $\delta_{30} = 1.2$ $\delta_{40} = 0.4$

1250−102	0.0143
1251−122	0.0133
1258−321	0.0149
1333−337	0.0129

Group 7
$\bar{l} = 47°$ $\bar{b} = 44°$ $\bar{z} = 0.032$
$\delta_{20} = 11.9$ $\delta_{30} = 4.0$ $\delta_{40} = 1.6$

1549+202	0.0318
1601+173	0.0354
1602+240	0.0318
1602+178	0.0315
1615+351	0.0296
1626+396	0.0297
1652+398	0.0337
1658+302	0.0351

Group 8
$\bar{l} = 97°$ $\bar{b} = 33°$ $\bar{z} = 0.027$
$\delta_{20} = 6.0$ $\delta_{30} = 1.4$ $\delta_{40} = 0.3$

1557+708	0.0258
1637+826	0.0245
1744+557	0.0304
1754+626	0.0276
1755+626	0.0276

Group 9
$\bar{l} = 322°$ $\bar{b} = -23°$ $\bar{z} = 0.018$
$\delta_{20} = 4.1$ $\delta_{30} = 1.0$ $\delta_{40} = 0.4$

1637−771	0.0241
1718−649	0.0142
1814−766	0.0189
1833−772	0.0178
1941−554	0.0147

These statistics give an indication of the presence of significant structure on very large scales, but do not quantify the results in a very useful way. In Section 5, we approach the problem in a different way by means of a direct power-spectrum analysis of the radio-galaxy density field.

4.2 The Tully effect

Having shown that radio galaxies display a correlation approaching that of Abell clusters, it is interesting to compare with another aspect of the Abell cluster distribution. Tully (1986, 1987) has claimed that the distribution of rich clusters shows a marked flattening throughout the volume $z < 0.1$, in the sense of a concentration towards the supergalactic x–y plane (supergalactic Z points towards $\alpha = 283\overset{\circ}{.}188$, $\delta = 15\overset{\circ}{.}642$).

Tully's analysis took the observed SGZ distribution and attempted to renormalize it to allow for sample selection

(zone of avoidance and radial selection) in order to produce a plot of SGZ-dependent density. This procedure is a little dangerous in that it amplifies the statistical noise in the distribution at large distances from the plane. We therefore carry out our analysis by comparison of observed SGZ histograms, using the simulation procedures discussed above to estimate the expected SGZ distribution on the null hypothesis that the density field is isotropic.

We show the comparison for various redshift shells in Fig. 5. There is a clear concentration to the supergalactic plane for $z<0.02$, but nothing significant in the shells at higher redshift. We believe it was this flattening of the distribution at low redshifts which accounts for the concentration towards the supergalactic plane observed in the sky distribution of sources from the Molonglo survey (Shaver & Pierre 1989). On larger scales, we see no evidence for the sort of effect claimed by Tully, and therefore conclude that it is possible that his result derived from non-uniformity in the Abell catalogue.

5 POWER-SPECTRUM ANALYSIS

5.1 Techniques

Although it is a common tool, the correlation function may not be the best way of answering some questions about cosmic structure. In many ways, the power spectrum is a simpler quantity to consider; this measures directly the contribution of different scales to $\delta\rho/\rho$ – and is what we are supplied with by e.g. inflationary theories. Rather than attempting to Fourier transform the noisy estimate of $\xi(r)$, it is better to determine the power spectrum directly. This is particularly true on very large scales, where $\xi(r)$ is very sensitive to assumptions about the mean density (because $1+\xi\propto\bar{n}^{-1}$ and $\xi\ll 1$); a direct transform of the data, however, yields Fourier coefficients of $\delta\rho/\rho$ which scale directly with $\bar{n}^{-1}$. Power-spectrum analysis thus gives a more robust determination of the large-scale density field. Similar reasoning has been used by Baumgart & Fry 1991, who give a power-spectrum analysis of various optical galaxy catalogues; however, as detailed below, we believe that their analysis contains an error.

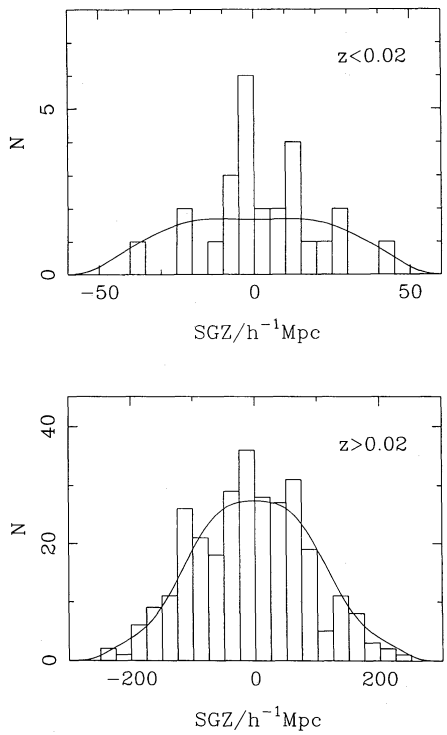

Figure 5. Histograms of supergalactic Z distance, for various redshift bands. The expected distribution for an isotropized catalogue with uniform sky coverage is shown as the smooth curve. There is no evidence for any concentration towards the supergalactic plane beyond $z=0.02$.

Our procedure needs to be a little different from that of Webster (1976). He used power-spectrum analysis as a statistical test for departures from randomness, whereas we are actually hoping to *quantify* such deviations. However, let us start by following Webster and considering N galaxies which are randomly and uniformly distributed throughout a cube of volume V. In the continuum case, we would like to evaluate the Fourier coefficients

$$\delta_k=\frac{1}{V}\int\delta(\boldsymbol{x})\exp i\boldsymbol{k}\cdot\boldsymbol{x}\,d^3x, \tag{10}$$

where δ is shorthand for $\delta\rho/\rho$, not the Dirac δ function; k denotes *comoving* wavenumber ($k=2\pi/\lambda$). Here, $|\delta_k|^2$ would be the true power spectrum of the density perturbation field in the sampled region of space. We need to form an estimator for this quantity, which will be denoted by $|\hat{\delta}_k|^2$. Note that the ideal $|\delta_k|^2$ may differ from the global average over a large volume; in what follows, we assume that the volume to hand is large enough to form a fair sample of the Universe. For the case of a limited number of galaxies sampling the density field, we estimate Fourier coefficients by the direct sum

$$a_k\equiv\sum_i N^{-1}\exp i\boldsymbol{k}\cdot\boldsymbol{x}_i. \tag{11}$$

In the absence of clustering, these coefficients execute a random walk on the Argand plane. The expectation value of the power is evaluated by splitting 3D space into a large number of cells with occupation numbers $n_i=0$ or 1 (*cf.* Peebles 1980)

$$\langle|a_k|^2\rangle=\sum_i n_i^2/N^2=1/N. \tag{12}$$

For $N\gg 1$ the central limit theorem yields the Rayleigh distribution for a single mode:

$$P(|a_k|^2>X)=\exp-NX. \tag{13}$$

This is the distribution of 'Poisson noise' which will overlay the true clustering signal that we are trying to measure.

If there are any true non-zero Fourier coefficients in the distribution of points, it is easy to see that the true and Poisson powers approximately add:

$$\langle|a_k|^2\rangle=\sum_i n_i^2/N^2+N^{-2}\left\langle\sum_i\sum_{i\neq j}\exp i\boldsymbol{k}\cdot(\boldsymbol{r}_i-\boldsymbol{r}_j)\right\rangle \tag{14}$$

$$=\frac{1}{N}+\frac{N-1}{N}|\delta_k|^2_{\rm true}$$

Thus, the power-spectrum estimator in this simplest case is (for large N)

$$|\hat{\delta}_k|^2 = |a_k|^2 - 1/N. \tag{15}$$

If we consider a system periodic on the scale $V^{1/3}$, then the power contributed by modes in a given region of k space is approximated in the continuum limit by $V/(2\pi)^3 \int |\delta_k|^2 \, d^3k$, where $V/(2\pi)^3$ is the usual density of states. As we change the box size, this integral must be held fixed; any true power in a given discrete mode will therefore scale proportional to V^{-1}, owing to the variation of the density of states with V. Thus, since the Poisson noise is $1/N$ per mode, the 'signal-to-noise' just depends on the background number density of points:

$$|\delta_k|^2_{\text{true}} / |\delta_k|^2_{\text{Poisson}} \propto n_b. \tag{16}$$

Now, since in practice we have a region of space in which the density is not constant, this suggests that we ought to weight contributions to mode amplitudes according to the expected background density (the usual reciprocal variance weighting):

$$\frac{1}{V}\int \delta(\boldsymbol{x}) \exp i\boldsymbol{k}\cdot\boldsymbol{x}\, d^3x \rightarrow \frac{1}{\langle n_b\rangle V}\int n_b(\boldsymbol{x})\, \delta(\boldsymbol{x}) \exp i\boldsymbol{k}\cdot\boldsymbol{x}\, d^3x. \tag{17}$$

Conveniently, this is almost what happens when we simply transform the observed pattern of points:

$$\frac{1}{\langle n_b\rangle V}\int n_b(\boldsymbol{x})[1+\delta(\boldsymbol{x})] \exp i\boldsymbol{k}\cdot\boldsymbol{x}\, d^3x \rightarrow \sum_i N^{-1} \exp i\boldsymbol{k}\cdot\boldsymbol{x}_i. \tag{18}$$

With larger data sets, the density might reach the point where one would wish to downweight the contributions from high-density regions on the grounds that true sampling fluctuations were dominating Poisson noise. In this case, the density weighting could be modified to introduce a critical density above which all volumes are weighted equally: $n_b \rightarrow (n_b^{-1} + n_c^{-1})^{-1}$. We shall not do this here, as the results below show that Poisson noise does indeed dominate in the present sample.

The Fourier coefficients produced by a direct transform of the data differ from the ideal case (a uniformly sampled very large cubical survey) in three distinct ways, which must be corrected for. Suppose a varying background is produced by selection of some varying fraction of objects, $n_b = f(\boldsymbol{x})\,\bar{n}$. The corrections this introduces are, in outline.

(i) The Fourier coefficients obtained are proportional to the transform of $f(\boldsymbol{x})[1+\delta(\boldsymbol{x})]$, so the transform of f needs to be subtracted.

(ii) The selection function has a smaller effective volume than any cube in which it is embedded, which affects the amplitude of the power spectrum.

(iii) Modes of large wavelength are spuriously reduced in amplitude because the mean density is estimated from the sample itself.

We first need to subtract the transform of the selection function, $f(\boldsymbol{x})$, which vanishes in the usual case of a uniform distribution:

$$b_k \equiv \sum_i N^{-1} \exp i\boldsymbol{k}\cdot\boldsymbol{x}_i - \frac{1}{N}\int n_b(\boldsymbol{x}) \exp i\boldsymbol{k}\cdot\boldsymbol{x}\, d^3x. \tag{19}$$

We can now subtract the Poisson contribution $\langle |b_k|^2\rangle = 1/N$ from the power (neglecting the factor $[N-1]/N$). If Poisson noise dominates, and if the selection function has little structure at large k, it may seem that the properties proved by Webster (1976) should still hold: different b_k should be uncorrelated and the result of summing over a shell in k space containing m modes should be an approximately Gaussian variable with variance $2m/N^2$ (the reality of the density field means that $\delta_k(-\boldsymbol{k}) = \delta_k^*(\boldsymbol{k})$; only half the modes in a shell are independent, hence the factor 2). The quantity

$$\hat{P}(k) \equiv \sum_k |b_k|^2 - \frac{m}{N} \tag{20}$$

might therefore seem to be a good candidate for an estimator of any true power in a shell of k space containing m modes, with an approximate error bar of $\sqrt{2m}/N$. However, we have yet to deal with normalization corrections.

The Fourier coefficients b_k produced in the above way are (to within noise) the convolution of the true δ_k with the transform of the selection function, and some care is needed in analysing the effect of this process on the power spectrum. Each mode we deduce is a sum over all true modes: $(b_k)_i = \Sigma\, W(i,j)(\delta_k)_j$. The new power spectrum therefore consists of a convolution between the power spectra of the density field and selection function ($|b_k|_i^2 = \Sigma\, |W|^2(i,j)\, |\delta_k|_j^2$), plus cross terms. However, the cross terms will clearly be zero on average, even if the different δ_k modes are correlated, provided there is not also a correlation between the phases of the selection function transform and the δ_k. This is just equivalent to the assumption that the sample is fair, and is not biased by e.g. excluding the region around all rich clusters. Our estimator is thus for the quantity $|\delta_k|^2 * |f_k|^2$ which we shall denote by $|\delta_k|^2_*$. With the exception of very low k (see below), this convolution has a negligible effect on the shape of the power spectrum, because the selection function contains relatively little small-scale power. However, it does affect the normalization in two ways: (i) the total number of objects, N, used to normalize changes from $\bar{n}\int d^3x$ to $\bar{n}\int f\, d^3x$; (ii) the area under the power spectrum of the selection function, $|f_k|^2$, changes by a factor $\int f^2 d^3x / \int d^3x$ (by Parseval's theorem). Thus, $\hat{P}(k)$ must be scaled to account for these changes:

$$\hat{P}(k) \rightarrow \hat{P}(k)\, \frac{[\int f\, d^3x]^2}{\int f^2 d^3x \int d^3x}. \tag{21}$$

If f is normalized so that $\int f d^3x = 1$ then, for a discrete grid in k space, this becomes simply

$$\hat{P}(k) \rightarrow \hat{P}(k) \Big/ \sum_{k=0}^{k_{\max}} |f_k|^2. \tag{22}$$

To sum up the steps required in the analysis so far, the final estimator for the true power spectrum convolved with $|f_k|^2$ is

$$|\hat{\delta}_k|^2_* = [|b_k|^2 - 1/N] \Big/ \sum_{k=0}^{k_{\max}} |f_k|^2, \tag{23}$$

where the coefficients b_k are defined by equation (19).

A useful check that this procedure gives a sensible answer is to consider the case of a uniform cubical survey of volume V embedded in a larger cube of volume V': use of the density of states for the larger volume gives $\hat{P}(k)$ too high by a factor V'/V. The analysis of Baumgart & Fry (1991) appears to be faulty at this point. They scale power spectra from

samples of different volume by a factor V^2/V'^2 rather than V/V', thereby deducing a power spectrum which increases spuriously with increasing sample depth. Thinking of the correction factor in this way as an incorrect counting of modes, we see that the errors bars on $\hat{P}(k)$ do not scale in the same way as $\hat{P}(k)$ itself. The errors are proportional to $\sqrt{m}$, where there are m modes in the region of k space under consideration, and hence should be scaled by only the square root of the factor which applies to $\hat{P}(k)$ itself.

Finally, there are more subtle normalization effects arising because the mean density is unknown and the condition $\langle\delta\rangle=0$ is applied to the data. This can clearly cause a systematic underestimate of power in modes whose wavelengths approach the size of the sample volume. Similar problems exist in estimating the correlation function within a finite volume, but are much more severe in that case. The combination $1+\xi$ is inversely proportional to the mean density; for finite samples, this can be significantly affected by modes larger than the sample size. This means that it is impossible in practice to measure ξ when it drops below the fractional uncertainty in the mean density. With the power spectrum, the main effect of such an offset in mean density is just to scale the amplitudes of all modes by some factor. However, the relative amplitude of large-wavelength modes is also affected, as follows. We shift the true DC level of δ by subtracting the mean value over our sample:

$$\delta' = \delta - \int \delta(\boldsymbol{x}) f(\boldsymbol{x})\, d^3x. \tag{24}$$

In what follows, we will need to distinguish carefully between the power spectrum of the true density field, $P(k)$, and the power spectrum of the renormalized field (P'), together with their convolved counterparts (P_* and P'_*). The DC shift is close in appearance to the case where a baseline consisting of the convolution $\delta * f$ is subtracted, which would be easy enough to correct for, since $P(k)=P'(k)/|1-f_k|^2$. More accurately, the subtraction of a constant offset is equivalent to forcing the power spectrum at $k=0$ to be zero, by subtracting a spike at the origin. Since we have established that the power spectrum we estimate is the true one convolved with $|f_k|^2$, the spike is also convolved over and we have $P'_*(k)=P_*(k)-P_*(0)|f_k|^2$, i.e.

$$P'_*(k) = P_*(k)\left[1-|f_k|^2\frac{P_*(0)}{P_*(k)}\right]. \tag{25}$$

The effect that this has depends on the power spectrum; consider power-law spectra with $|\delta_k|^2 \propto k^n$. Clearly, for an $n=0$ spectrum, the 'normalization damping' factor is just $(1-|f_k|^2)$; only modes with $|f_k|^2 \gtrsim 0.1$ will be affected at all significantly. Some numerical experiments at convolution of different power laws with Gaussian $|f_k|^2$ functions show that this statement holds reasonably well for all realistic values of n. For spectra with $P(0)=0$ (i.e. $n>0$), the convolution process produces spurious power at $k=0$, which is removed by the above process. The net result can be that $P'_*(k)$ is actually closer to the true $P(k)$ than is $P_*(k)$. On this basis, we expect that normalization corrections will be at most 10–20 per cent for the largest wavelengths investigated below, and these effects have therefore been neglected in what follows.

For completeness, we should also cover the possibility that the estimation of the radial part of the selection function from the observed redshift distribution may introduce a bias in the power spectrum. This would certainly be the case with pencil-beam surveys over a restricted sky area, where most of the clustering signal comes from clumping in redshift. However, one of the advantages of having all-sky coverage is that the sample is immune to such problems. Consider a fluctuation of very long wavelength: this will appear as a simple dipolar density gradient in the data, but it will have no effect whatsoever on the redshift distribution deduced by averaging over radial shells. There will therefore be no tendency to underestimate power in very long-wavelength fluctuations. To the extent that our sample has very nearly uniform all-sky coverage, any such effects should be of a higher order than those discussed above.

To present the results, it will be convenient to use the notation

$$\Delta^2 \equiv \frac{V}{(2\pi)^3} 4\pi k^3 |\delta_k|^2, \tag{26}$$

i.e. Δ^2 is the contribution to the fractional variance from unit range of $\ln k$. This is obtained from $|\hat{\delta}_k|^2_*$ just by adding power from shells in k space, and dividing by the appropriate bin size in $\ln k$. In these terms, the usual definition of a power-law power spectrum becomes $\Delta^2 \propto k^{3+n}$.

5.2 Tests on simulated data

The above procedure is somewhat involved by comparison with the estimation of $\xi(r)$. It therefore seems important to carry out a test on a mock data set. Accordingly, we created a density field with the power spectrum characteristic of $\xi=(r/11\ h^{-1}\ \mathrm{Mpc})^{-1.8}$ clustering (see below). This was achieved by generating a realization of a Gaussian field $G(\boldsymbol{x})$ and adjusting its power spectrum empirically until the lognormal field $\exp(G)$ had the desired power spectrum. Apart from enforcing positively, this model may be a reasonable representation of observed galaxy clustering (Coles & Jones 1991). This density field was then multiplied by a selection function to censor $|b|<15°$ and produce an expected redshift distribution dn/dz constant for $0.01<z<0.1$, and a mock sample of size equal to the true one was selected Poissonianly from the resulting field. The sky distribution of this mock data set is shown in Fig. 6. It is interesting that the large-scale distribution of the true data seems rather more uniform. As we shall see, this is a hint of a lack of power on very large scales in the radio galaxy sample.

Fig. 7 shows the initial stages in the analysis procedure as applied to the mock data: (a) the raw power spectrum of the data; (b) the power spectrum after subtraction of the Fourier transform of the selection function from that of the data; (c) the result after subtraction of the Poisson contribution. These results used a 64^3 FFT in practice, with a box side of 558 h^{-1} Mpc (i.e. covering space out to $z=0.1$). For this size of array, the points of highest k are just starting to be affected by binning, but this is a small correction (see Baumgart & Fry 1991). The main points to note are how effectively the spurious signal at low k in the raw data is removed, plus the fact that Poisson noise is rather larger than the remaining signal.

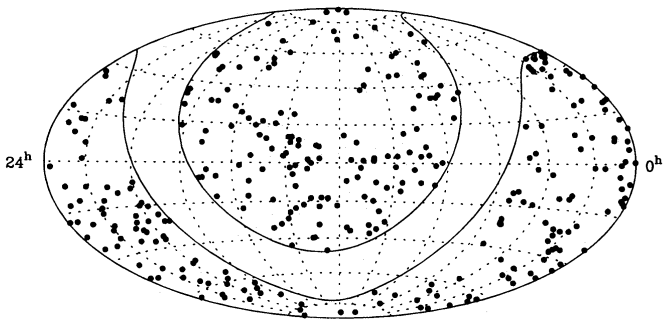

Figure 6. The sky distribution of a realization of a mock catalogue designed to have the same sky coverage and redshift distribution as the true data (*cf.* Fig. 1a). The simulation is a lognormal model with a power-law correlation function $\xi=(r/11\ h^{-1}\ \mathrm{Mpc})^{-1.8}$ and no long-wavelength cut-off. Even in the sky distribution, some indication of the large-scale power may be seen in the form of a large angular void.

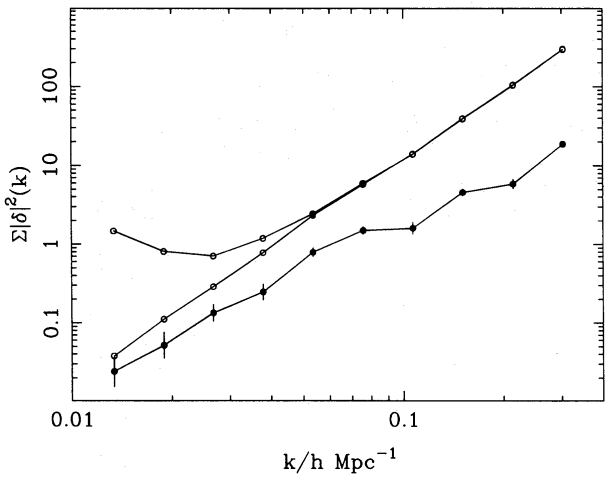

Figure 7. Illustrating the determination of the power spectrum, for the mock data set. We show the raw power in each bin of k space (of full width 0.35 in ln k), uncorrected for bin size or for the effects of selection-function convolution (upper set of open circles), then the data with the selection function transform subtracted (lower set of open circles), then the final answer with the Poisson power removed (filled points). Note that the Poisson power dominates over the true signal, except in the first few bins.

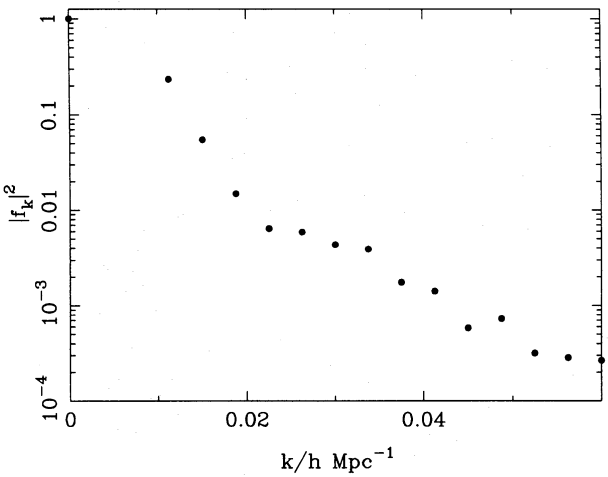

Figure 8. The Fourier transform of the selection function for the mock data, $|f_k|^2$. At long wavelengths, this resembles a Gaussian $f_k=\exp[-(kR_f)^2/2]$ with $R_f\simeq 100\ h^{-1}$ Mpc.

It now remains to apply the corrections for the selection function detailed above. Fig. 8 shows $|f_k|^2$ for the mock sample, which is very close in appearance to that of the true data, as intended. At low k, the function resembles a Gaussian filter with $R_f\simeq 100\ h^{-1}$ Mpc. This implies that modes with $k\simeq 0.015\ h$ Mpc^{-1} will have their power reduced by about 10 per cent by normalization effects; modes of much smaller k are very significantly affected, and so this sets the limit on the wavelengths we can investigate.

Applying the corrections as above and converting $P(k)$ into $\Delta^2(k)$ by dividing by the bin size in ln k yields the final estimate for the power spectrum, which is shown in Fig. 9. The dashed line shows the expected power spectrum, which is reproduced gratifyingly well, even out to the largest wavelengths. The Poisson error bars seem of a realistic size for $\lambda>100\ h^{-1}$ Mpc, but appear to be a little too small for smaller wavelengths, where a scatter in power of 10–20 per cent seems to apply. It is to be expected that sampling effects would reveal themselves in these bins: as k increases, the number of modes in a bin of ln k rises as k^3, so that the Poisson errors rapidly tend to zero and reveal any additional scatter caused by sampling a clustered distribution. Note that this is the opposite of the behaviour which applies for the correlation function: there, the Poisson error bars become progressively less realistic at *large* scales.

5.3 Power-spectrum results

We now apply the same analysis to the real data. Fig. 10 shows the final result: the fully corrected power spectrum for the $z<0.1$ sample. Where the power is not significantly non-zero, we plot 90 per cent confidence upper limits. Taking these into account, we see that significant curvature of the power spectrum exists, with a break at $\lambda\sim 200\ h^{-1}$ Mpc. This conclusion is confirmed by Webster's (1976) limit at larger wavelengths, which also falls below an extrapolation of the power-law spectrum at large k. The power-spectrum index for $\lambda\gtrsim 200\ h^{-1}$ Mpc must be $n\gtrsim -0.5$.

This break in the spectrum is on scales quite close to the limit of the sample, so it is reassuring that the simulated data

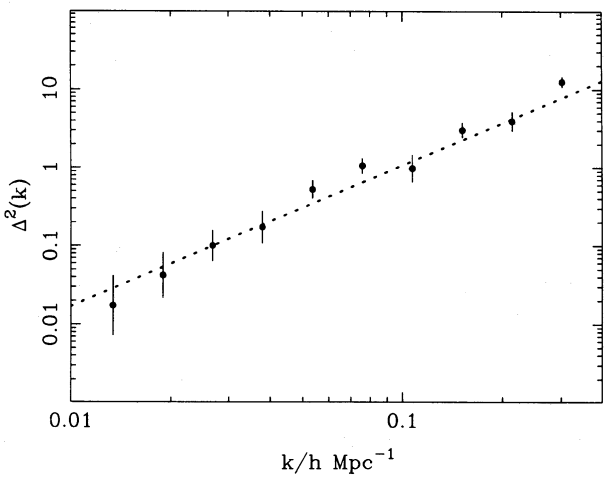

Figure 9. The final corrected power spectrum for the mock data, correcting Fig. 7 for bin size in k space and the volume of the selection function. The dotted line shows the input assumed power-law power spectrum, which is recovered in a very satisfactory manner.

set did show that clustering on these scales could be detected, if present at the level required by the absence of a break. Only one realization of the simulated data was discussed in Section 5.2, but other realizations were run and these confirm that we do not expect results as low as those observed in the absence of a break. Both Figs 9 and 10 were produced using the assumption of uniform sky coverage to generate the random catalogues, so there should have been no tendency to suppress that part of the clustering signal which comes from the sky distribution. We can attempt to gain a little extra information by extending the sample limit to $z=0.15$. The survey was not intended to be complete to this limit, but we can proceed by assuming that the incompleteness is some isotropic radial function. If this assumption is false, it can only add spurious large-scale power. This analysis used only measured redshifts, yielding a sample of 374 objects. The power spectrum is shown in Fig. 11. The appearance is similar to that of Fig. 10, although the depth (as measured by the width of $|f_k|^2$) has increased by about 15 per cent.

As one further test on the reality of the clustering, we have investigated the isotropy of the signal by looking at the power spectra estimated from independent quadrants of k space. This confirms that the signal does not arise from some special directions. Our result is not due to improper allowance for anisotropies in the selection function.

We have compared the results with two analytical models. Suppose the two-point correlation function to be an exact power-law:

$$\xi(r)=(r/r_0)^{-\gamma}. \tag{27}$$

The corresponding power spectrum expressed in terms of variance per unit ln k is

$$\Delta^2\equiv\frac{V}{(2\pi)^3}4\pi k^3|\delta_k|^2=\frac{2}{\pi}(kr_0)^\gamma\Gamma(2-\gamma)\sin\frac{(2-\gamma)\pi}{2} \tag{28}$$

$[=0.903(kr_0)^{1.8}$ if $\gamma=1.8]$. The 'standard model' of galaxy clustering has long been one with $\gamma=1.8$, $r_0=5\ h^{-1}$ Mpc. However, we do now have some evidence that this overpredicts the power spectrum at large wavelengths. The strongest case for this probably comes from the $w(\theta)$ results of the APM galaxy survey (Maddox *et al.* 1990). Their data can be described by the following power spectrum (Peacock 1991)

$$\Delta^2(k)=\frac{0.039y^4}{(1+y^{2.4})};\qquad y\equiv k/0.025\ h\ \mathrm{Mpc}^{-1}. \tag{29}$$

This gives a break from an effective $n=-1.4$ to the scale-invariant $n=1$ at around $\lambda=200\ h^{-1}$ Mpc. If we make the reasonable assumption that the power spectrum of our radio galaxies is at all wavelengths a scaled version of that for galaxies in general (Kaiser 1984), then we see from Fig. 11 that our present results are well consistent with the above model for the APM power spectrum, scaled up by a factor of about 3.

It is worth noting once again the superiority of the power-spectrum approach. The correlation function corresponding to the above model for $\Delta^2(k)$ has a break at $r\simeq 30\ h^{-1}$ Mpc. A glance at Fig. 3 shows that it would be rather hard to distinguish between the presence or absence of this break given the fluctuations in $\xi(r)$ at large r.

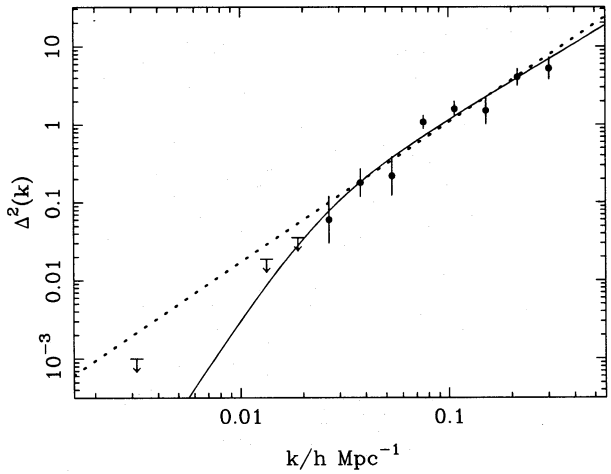

Figure 10. The final corrected power spectrum for the sample. Where the power was not significantly detected according to the Poisson errors, we plot 90 per cent confidence upper limits. The upper limit at smallest k is the result from Webster (1977). The two lines show the two models for galaxy clustering described in the text. The dotted line extrapolates the small-scale clustering: $\xi=(r/11\ h^{-1}$ Mpc$)^{-1.8}$, whereas the solid line is the functional form which describes the APM $w(\theta)$, scaled vertically by a factor 3.3. We can clearly rule out continued power-law clustering on large scales, but the power spectrum which describes the APM $w(\theta)$ appears well consistent with the data.

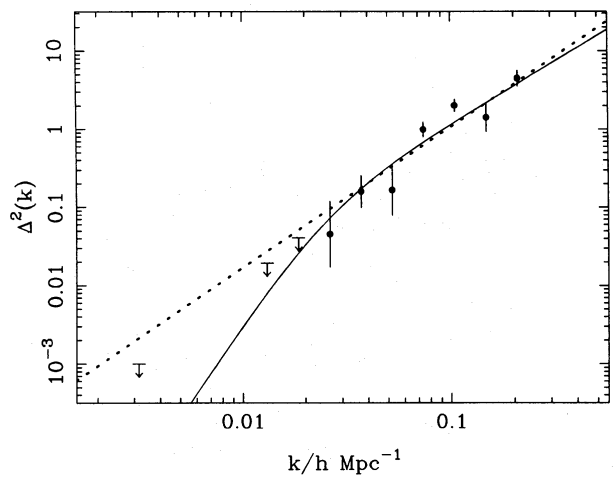

Figure 11. As for Fig. 10, but including data out to $z=0.15$. This increases sample size and (more importantly) depth by about 15 per cent. The appearance is very similar to Fig. 10; this gives some added confidence that the reduction in power at small k is not due to systematic effects near the sample volume limit. Although the sample is incomplete beyond $z=0.1$, it appears that this incompleteness does not vary strongly over the sky, since no new large-scale power is detected.

6 SUMMARY AND CONCLUSIONS

We have extended Webster's classical work on the clustering of radio galaxies, using a redshift survey to look at spatial correlations without the reduction in sensitivity caused by

projection effects. As a result, we have been able to make the first detection of small-scale clustering in these objects. The derived clustering length, $r_0 = 11\ h^{-1}$ Mpc, is in reasonable accord with the nature of radio galaxies: luminous elliptical galaxies inhabiting moderate to rich environments are certainly expected to show enhanced correlations of this order.

We have been unable to reproduce any strong tendency for clustering to depend on radio power, which had been suggested by the analysis of an earlier, incomplete, version of this sample. In retrospect, this may not be too surprising as the evidence for any strong radio-luminosity dependence of environmental richness is not as strong as it once appeared.

Having established radio galaxies as valid probes of galaxy clustering, we turned to a direct power-spectrum analysis in the hope of constraining clustering on the largest scales. There appears to be evidence for a break in the power spectrum at wavelengths $\lambda \sim 200\ h^{-1}$ Mpc. At shorter wavelengths, the spectrum is consistent with a power law of effective index $n \simeq -1.4$, but this has to break to $n \gtrsim -0.5$ for larger wavelengths. Clearly, there is some way to go before one can claim to have produced evidence for scale invariance on the largest scales, but it is encouraging that both this and other pieces of work are starting to point in the same direction. At last, after years when each increase of sample depth seemed to show ever larger structures in the galaxy distribution, the process may be converging. If we adopt a universal power scaling factor of 3, then our results imply $\Delta^2 \simeq 0.1$ at the $128\ h^{-1}$ Mpc scale singled out by the pencil-beam survey of Broadhurst *et al.* (1990). If this number is to be taken seriously, then one would be forced to conclude that the behaviour seen in the Broadhurst *et al.* survey is not the result of very large inhomogeneities on these scales, and other explanations must be sought (e.g. Kaiser & Peacock 1991). We note that other redshift surveys attempting to settle this question must take into account the very large wavelengths which are under dispute: depths of several hundred Mpc are required to probe the scales of interest.

We may hope that the question of the very large-scale power spectrum of galaxy clustering will be settled in the next few years, as cosmic background radiation experiments such as *COBE* place stronger constraints on the Gpc-scale spectrum. The next step will be to constrain the statistics of the fluctuations, to test for the inflationary requirement that they be Gaussian. We are probably close to possessing sufficient data in deep samples to be able to address this question.

ACKNOWLEDGMENTS

We are extremely grateful to our observational collaborators on the radio-galaxy redshift survey, Chris Collins, Simon Lilly and Lance Miller, without whom this analysis would not have been possible. We thank Tom Broadhurst for helpful discussions. Part of this work was performed while JAP was a visiting fellow at the Canadian Institute for Theoretical Astrophysics, and their hospitality is gratefully acknowledged. DN was supported by a SERC postgraduate studentship.

REFERENCES

Auriemma, C., Perola, G. G., Ekers, R., Fanti, R., Lari, C., Jaffe, W. J. & Ulrich, M.-H., 1977. *Astr. Astrophys.*, **57,** 41.
Bahcall, N. A. & Soneira, R., 1983. *Astrophys. J.*, **270,** 20.
Bahcall, N. A. & Soneira, R., 1984. *Astrophys. J.*, **277,** 27.
Baumgart, D. J. & Fry, J. N., 1991. *Astrophys. J.*, **375,** 25.
Bolton, J. G., Wright, A. E. & Savage, A., 1979. *Aust. J. Phys. Astrophys. Suppl.*, **46.**
Broadhurst, T. J., Ellis, R. S., Koo, D. C. & Szalay, A. S., 1990. *Nature,* **343,** 726.
Cohen, A. M., Porcas, R. W., Browne, I. W. A., Daintree, E. J. & Walsh, D., 1977. *Mem. R. astr. Soc.*, **84,** 1.
Coles, P. & Jones, B., 1991. *Mon. Not. R. astr. Soc.*, **248,** 1.
Day, G. A., Shimmins, A. J., Ekers, R. D. & Cole, D. J., 1966. *Aust. J. Phys.*, **19,** 35.
Davis, M. & Geller, M. J., 1976. *Astrophys. J.*, **208,** 13.
Fanaroff, B. L. & Riley, J. M., 1974. *Mon. Not. R. astr. Soc.*, **167,** 31P.
Grueff, G. & Vigotti, M., 1972. *Astr. Astrophys. Suppl.*, **6,** 1.
Grueff, G. & Vigotti, M., 1973. *Astr. Astrophys. Suppl.*, **11,** 41.
Grueff, G. & Vigotti, M., 1979. *Astr. Astrophys. Suppl.*, **35,** 371.
Hill, G. J. & Lilly, S. J., 1991. *Astrophys. J.*, **367,** 1.
Kaiser, N., 1984. *Astrophys. J. Lett.*, **284,** L9.
Kaiser, N., 1986. *Mon. Not. R. astr. Soc.*, **219,** 785.
Kaiser, N., 1987. *Mon. Not. R. astr. Soc.*, **227,** 1.
Kaiser, N. & Peacock, J. A., 1991. *Astrophys. J.*, in press.
Kühr, H., Pauliny-Toth, I. I. K., Witzel, A. & Schmidt, J., 1981. *Astr. J.*, **86,** 854.
Kühr, H., Johnston, K. J., Odenwald, S. & Adlhoch, J., 1987. *Astr. Astrophys. Suppl.*, **71,** 493.
Lilly, S. J. & Prestage, R. M., 1987. *Mon. Not. R. astr. Soc.*, **225,** 531.
Ling, E. N., Frenk, C. S. & Barrow, J. D., 1986. *Mon. Not. R. astr. Soc.*, **223,** 21P.
Longair, M. S. & Seldner, M., 1979. *Mon. Not. R. astr. Soc.*, **189,** 433.
Maddox, S. J., Efstathiou, G., Sutherland, W. J. & Loveday, J., 1990. *Mon. Not. R. astr. Soc.*, **242,** 43P.
Masson, C. R., 1979. *Mon. Not. R. astr. Soc.*, **187,** 253.
Mayer, C. J., 1979. *Mon. Not. R. astr. Soc.*, **186,** 99.
Owen, F. N. & Laing, R. A., 1989. *Mon. Not. R. astr. Soc.*, **238,** 357.
Peacock, J. A., Miller, L., Collins, C. A., Nicholson, D. & Lilly, S. J., 1988. In: *Large Scale Structures of the Universe, Proc. IAU Symp. No. 130,* p. 579, eds Audouze, J., Pelletan, M.-C. & Szalay, A., Kluwer, Dordrecht.
Peacock, J. A., 1991. *Mon. Not. R. astr. Soc.*, in press.
Peebles, P. J. E., 1973. *Astrophys. J.*, **185,** 413.
Peebles, P. J. E., 1980. *The Large-Scale Structure of the Universe,* Princeton University Press, Princeton.
Phillipps, S. & Shanks, T., 1987. *Mon. Not. R. astr. Soc.*, **229,** 621.
Porcas, R. W., Urry, C. M., Browne, I. W. A., Cohen, A. M., Daintree, E. J. & Walsh, D., 1980. *Mon. Not. R. astr. Soc.*, **191,** 607.
Prestage, R. M. & Peacock, J. A., 1988. *Mon. Not. R. astr. Soc.*, **230,** 131.
Prestage, R. M. & Peacock, J. A., 1989. *Mon. Not. R. astr. Soc.*, **236,** 959.
Saunders, W., Frenk, C., Rowan-Robinson, M., Efstathiou, G., Lawrence, A., Kaiser, N., Ellis, R., Crawford, J., Xia, X.-Y. & Parry, I., 1991. *Nature,* **349,** 32.
Scaramella, R., Baiesi-Pillastrini, G., Chincarini, G., Vettolani, G. & Zamorani, G., 1989. *Nature,* **338,** 562.
Shaver, P. A. & Pierre, M., 1989. *Astr. Astrophys.*, **220,** 35.
Shimmins, A. J. & Day, G. A., 1968. *Aust. J. Phys.*, **21,** 377.
Subrahmanya, C. R. & Hunstead, R. W., 1986. *Astr. Astrophys.*, **170,** 27.
Sutherland, W., 1988. *Mon. Not. R. astr. Soc.*, **234,** 159.
Tully, R. B., 1986. *Astrophys. J.*, **303,** 25.
Tully, R. B., 1987. *Astrophys. J.*, **323,** 1.
Valls-Gabaud, D., Alimi, J.-M. & Blanchard, A., 1989. *Nature,* **341,** 215.

Waggett, P. C., Warner, P. J. & Baldwin, J. E., 1977. *Mon. Not. R. astr. Soc.*, **181**, 465.
Webster, A. S., 1976. *Mon. Not. R. astr. Soc.*, **175**, 61.
Webster, A. S., 1977. In: *Radio Astronomy and Cosmology, IAU Symp. No. 74*, p. 75, ed. Jauncey, D. L., Reidel, Dordrecht.
Windhorst, R. A., 1984. *PhD thesis*, University of Leiden.
Willis, A. G., Strom, R. G. & Wilson, A. S., 1974. *Nature*, **250**, 625.
Wills, D. & Bolton, J. G., 1969. *Aust. J. Phys.*, **22**, 775.
Yates, M. G., Miller, L. & Peacock, J. A., 1989. *Mon. Not. R. astr. Soc.*, **240**, 129.

APPENDIX A: SAMPLE SELECTION

The initial design constraints on this sample were to cover a volume which was large enough to form an indisputably fair sample of the Universe, and also to allow tests for streaming velocities to be carried out to greater depths. Given that the streaming samples extended to galaxies at $z \simeq 0.04$ and that Tully had suggested the existence of structure in the Abell cluster distribution on scales up to $z \simeq 0.1$, the limit of $z = 0.1$ seemed an appropriate choice. As will be seen, this corresponds to an apparent magnitude of $B \simeq 17$: one is still dealing with relatively bright galaxies, for which completeness in the optical identifications should be readily attainable. A lower distance limit should also be set: very nearby galaxies are lost from the radio surveys through over-resolution. Also, at low redshift, redshift is not a good distance estimator, which complicates three-dimensional studies. A lower limit of $z = 0.01$ was selected; it should be possible to make the sample selection reasonably homogeneous when only a factor of 10 in distance needs to be allowed for. Both from the point of view of obscuration, and because of the lack of radio surveys, the galactic plane must be avoided. To make the survey boundary relatively simple, the limit $|b| > 15°$ was imposed. The ideal is then to select over the remaining 9.3 sr galaxies with $0.01 < z < 0.1$ down to some uniform flux-density limit.

A1.1 Radio selection

The whole sky away from the galactic plane is covered at radio wavelengths by one of four surveys of roughly equivalent depth: Parkes at 2.7 GHz for $\delta \lesssim 24°$; Bologna at 408 MHz for $24° \lesssim \delta \lesssim 40°$; Jodrell Bank at 966 MHz for $40° \lesssim \delta \lesssim 70°$; and Bonn at 5 GHz for $\delta \gtrsim 70°$. All these surveys have had associated with them extensive optical identification programmes based on radio positions of accuracy generally $\lesssim 10$ arcsec. Galaxies well above the limit of the sky survey should have been noted as candidate identifications if present.

Parkes. The various parts of the Parkes 2.7-GHz surveys are summarized by Bolton, Wright & Savage (1979). At $|b| > 15°$, almost all regions at $\delta < 4°$ have been surveyed to a 2.7-GHz limit of 0.35 Jy or deeper. The only exceptions are a few regions where the closest approach to the galactic plane is further than 15°: the worst such point is at $\alpha = 17^h$, $\delta = -4°$, $|b| = 21.9°$. These regions total well less than 1 per cent of the survey area, and may safely be neglected. The situation at $\delta > 4°$ is more complicated; the direct 2.7-GHz survey is complete to only 0.6 Jy in this region. However, the zone $4° < \delta < 20°$ was surveyed to 2.5 Jy at 408 MHz by Day *et al.* (1966); the objects found were then remeasured at 2.7 GHz. Also, all 4C sources in this zone down to 3 Jy at 178 MHz were observed at 2.7 GHz by Wills & Bolton (1969). For a spectral index of 0.8, these searches should thus be complete to respectively 0.55 Jy and 0.34 Jy at 2.7 GHz. Finally, the zone $20° < \delta < 27°$ was surveyed to 1.5 Jy at 635 MHz by Shimmins & Day (1968), again with 2.7-GHz follow up, at which frequency the equivalent limit is 0.47 Jy.

Bologna. The Bologna B2 survey at 408 MHz covered the declination band $24° < \delta < 40.3°$ to a limit of 0.25 Jy. Careful optical identifications were carried out for sources brighter than 0.9 Jy in three papers by Grueff & Vigotti (1972, 1973, 1979). These cover a region which again is close to but not precisely $|b| < 15°$. The worst omission is an area around $\alpha = 22^h$, $\delta = 30°$, and the total area from our target zone which is not covered is about 0.2 sr.

Jodrell Bank. The 966-MHz Jodrell Bank survey covered $40.3° < \delta < 71°$ to a limit of 0.7 Jy at 966 MHz. Accurate radio positions (± 2 arcsec) were measured for the compact sources using an interferometer, and optical identifications for these were reported by Cohen *et al.* (1977). The more extended sources were identified by Porcas *et al.* (1980).

Bonn. A series of 5-GHz surveys covering most of the northern sky were carried out during the 1970s at Greenbank and Bonn. The deepest of these was the Bonn S5 survey, which covered $\delta > 70°$ to a completeness limit of 0.25 Jy (Kühr *et al.* 1981). The S5 survey is also the one for which the most detailed optical identification work has been carried out, using VLA maps to produce very reliable identifications (Kühr *et al.* 1987).

Giant sources. Even at $z > 0.01$, a few radio sources have such large angular sizes ($\gtrsim 10$ arcmin) that they are not easily recognised as a single object. Such objects have been added to the sample where known: 0503−286 (Subrahmanya & Hunstead 1986); 0744+559 (Willis, Strom & Wilson 1974); 0945+734 (Mayer 1979); 1029+569 (Masson 1979); 1637+826 (Waggett, Warner & Baldwin 1977). There are doubtless others, particularly in the southern hemisphere, but such objects must constitute a tiny incompleteness in the total sample.

A1.2 Flux-density limits

The above flux-density limits translate to the following figures at the 'average' frequency of 1.4 GHz, assuming a spectral index of 0.8: 0.59 Jy (Parkes); 0.33 Jy (Bologna); 0.52 Jy (Jodrell Bank); 0.69 Jy (Bonn). These are all of a very similar depth, with the exception of Bologna. This was therefore cut back to a limit of 1.2 Jy at 408 MHz (equivalent to 0.44 Jy at 1.4 GHz). The all-sky sample therefore approximates a sample complete to 0.5 Jy at 1.4 GHz.

A1.3 Optical selection

Given that we are interested in radio galaxies with $z < 0.1$, what is the appropriate optical limit? A plot of estimated B magnitude against z for objects of known redshift from the above surveys shows the relation $\log_{10}(z/0.1) = 0.2(B - 17)$, with a scatter of about 1 mag. To ensure reasonable com-

pleteness to the chosen limit of $z = 0.1$, therefore, a conservative limit of $B = 19$ for galaxies of unknown redshift was taken to define the initial sample. This yielded 125 galaxies of known redshift, plus 454 candidate sample members. We have pursued spectroscopy of the candidates, and now have a total of about 460 redshifts, of which 310 lie in the original target range of $0.01 < z < 0.1$. The full data will be presented in detail elsewhere (Nicholson *et al.*, in preparation).